Influence of Solvent Polarity and Hydrogen Bonding on the EPR Parameters of a Nitroxide Spin Label Studied by 9-GHz and 95-GHz EPR Spectroscopy and DFT Calculations

Rikard Owenius,*,† Maria Engström, and Mikael Lindgren†

IFM-Departments of Chemical Physics and Computational Physics, Linköping University, SE-581 83 Linköping, Sweden

Martina Huber

Huygens Laboratory, MAT Group, Leiden University, P.O. Box 9504, 2300 RA Leiden, The Netherlands

Received: May 3, 2001; In Final Form: September 5, 2001

The isotropic and anisotropic hyperfine coupling constants and *g*-values of the nitroxide spin label (1-oxyl-2,2,5,5-tetramethylpyrroline-3-methyl)methanethiosulfonate (MTSSL) were determined from 9-GHz and 95-GHz electron paramagnetic resonance (EPR) measurements in various solvents with a large distribution in polarity and proticity. The parameters A_{iso}, g_{iso}, A_{zz}, and g_{xx} of MTSSL were found to be sensitive to changes in solvent properties, where *A*-values increased and *g*-values decreased due to increased solvent polarity or proticity. A linear correlation was found for the isotropic (g_{iso}, A_{iso}) and anisotropic (g_{xx}, A_{zz}) parameters, respectively. Furthermore, density functional theory (DFT) calculations of the same parameters were performed for a model spin label with the possibility to vary the dielectric constant (ϵ) of the medium and the number of hydrogen bonds formed with the nitroxide oxygen. From a qualitative analysis of experimental and calculated results, it was possible to specify the causes of the parameter shifts in more detail. In the "apolar region" ($\epsilon < 25$), the sensitivity of A_{iso} and A_{zz} to ϵ is large. However, in the "polar region" ($\epsilon > 25$), the sensitivity to ϵ is small, and the shifts in A_{iso} and A_{zz} are mainly determined by the proticity of the solvent. Methanol was found to form ∼1 and water ∼2 hydrogen bonds to the nitroxide on average. The DFT method determined the shifts in g_{iso} and g_{xx} due to hydrogen bonding more accurately compared with the restricted open-shell Hartree−Fock method. The anisotropic spin label-solvent data can be used in the interpretation of rigid-limit data from spin-labeled proteins to gain further insight in local environmental properties.

1. Introduction

Nitroxide spin labels are widely applied in combination with electron paramagnetic resonance (EPR) spectroscopy to investigate the structure and dynamics of proteins.[1,2] When a spin label is attached to a specific site of a protein, it is subjected to motional restrictions due to sterical constraints and interactions with surrounding structures. Since the EPR spectrum is highly sensitive to the mobility of the spin label, information about the local environment of the label can be obtained.

Apart from the sensitivity of the EPR technique to the motion of the spin label, the different EPR parameters associated with a spin label show a solvent dependence. This has been shown for the isotropic *g*-value (g_{iso}) and hyperfine coupling constant (A_{iso}),[3,4] as well as for the anisotropic *g*-tensor and hyperfine coupling (*A*) tensor.[5−7] The *g*-tensor component directed along the NO bond, g_{xx}, and the *A*-tensor component directed along the π orbital of the nitroxide radical (perpendicular to the plane of the ring structure), A_{zz}, are most sensitive to the polarity of the local environment and to interactions with surrounding molecules. The values of g_{xx} and A_{zz} also depend on the chemical structure of the nitroxide spin label.[8] Lebedev and co-workers observed a linear correlation between g_{xx} and A_{zz} of nitroxide spin labels, where g_{xx} decreases and A_{zz} increases with increased solvent polarity,[5,6] in accordance with an earlier study of g_{iso} and A_{iso}.[3] The EPR parameters are not only affected by the solvent polarity but also by hydrogen bonding to the oxygen atom of the nitroxide, which contributes significantly to g_{iso}, A_{iso}, g_{xx}, and A_{zz} if the radicals are dissolved in protic solvents, such as water or methanol.[3−6,9] The variation in A_{zz} seen from rigid-limit EPR measurements at 35 GHz on phospholipid bilayers was interpreted as a polarity gradient due to the nature of the bilayer.[4] A more detailed study of the *g*- and *A*-tensors, performed at 250 GHz on spin-labeled lipids, yielded lower g_{xx}- and higher A_{zz}-values when moving the spin label from the hydrophobic region to the polar headgroup of the phospholipid membrane.[7] These changes were attributed to differences in polarity along the lipid chain due to different degrees of water penetration. Thus, nitroxide spin labels are applicable as probes of local polarity in investigations of membranes. It is likely that they have similar applicability in structural and functional studies of globular proteins, as a complementary method to the probing of spin label motion. The spin label (1-oxyl-2,2,5,5-tetramethylpyrroline-3-methyl)methanethiosulfonate (MTSSL) is commonly used in studies of protein structure and dynamics.[2] Recently, MTSSL was also used as a probe of polarity in studies of the proton channel of the transmembrane proton pump bacteriorhodopsin at 9 GHz[10] and with enhanced sensitivity and spectral resolution at 95 GHz.[11]

* Corresponding author. Dr. Rikard Owenius, IFM-Department of Chemical Physics, Linköping University, SE-581 83 Linköping, Sweden. Phone: +46-13-282484. Fax: +46-13-288969. E-mail: rikow@ifm.liu.se.

† Present addresses. R. Owenius: Department of Chemistry and Biochemistry, University of Denver, 2190 E. Iliff Ave., Denver, CO 80208. M. Lindgren: Division of Sensor Technology, Swedish Defence Research Agency, P.O. Box 1165, SE-581 11 Linköping, Sweden.

10.1021/jp0116914 CCC: $20.00
Published on Web 11/10/2001

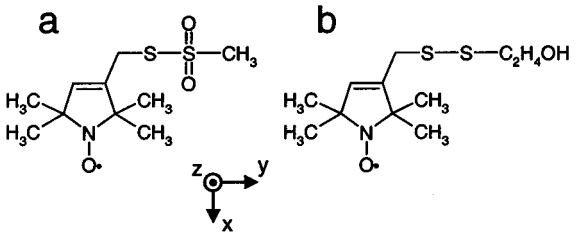

Figure 1. Structures of the spin labels used. (a) MTSSL and (b) MTSSL with β-mercaptoethanol covalently bound to it. The coordinate system defines the principal axis system of the magnetic tensors of the nitroxide radical.

The present paper is part of a combined theoretical and experimental work, which aims to assess the sensitivity of a specific spin label to various types of solvents and clarify the influence of solvent polarity and proticity on the response of the spin label. The response of the EPR parameters to different solvents, protic and aprotic within a range of 2.4 to 109 in dielectric constant, was examined for MTSSL and MTSSL−β-mercaptoethanol (Figure 1) using 9-GHz and 95-GHz EPR. Two kinds of solvent effects on the isotropic and anisotropic *g*- and *A*-tensor components of MTSSL were considered from solution and rigid-limit EPR spectra: (1) electrostatic effects due to the polarity of the solvent and (2) hydrogen bonding to the oxygen atom, as suggested by Griffith et al.[4] To obtain a deeper understanding of these effects, the experimental results were compared with density functional theory (DFT) calculations of the *g*- and *A*-tensors for a truncated model of MTSSL (MSL), where the linker is not included,[12] in different environments. DFT calculations of the *A*-tensor of radicals are widely used for different applications.[13−15] Rega et al. made DFT calculations on H_2NO radicals using the polarizable continuum model (PCM) and concluded that the PCM results were satisfying except in the case of protic solvents, such as water and methanol.[16] Semiempirical calculations have frequently been used for *g*-value calculations.[17−19] Recently, DFT[20−22] and ab initio[23−25] methods were developed. Calculations of *g*-values and hyperfine couplings of nitroxide spin labels in different environments are, however, rarely found in the literature. The influence of the geometric structure on the *g*-tensor of several nitroxide radicals was earlier investigated by semiempirical INDO methods.[26] It was found that g_{xx} is sensitive to variations in the geometrical parameters of the NO group, but the effect of remote substituents is relatively small. Recently, the influence of hydrogen bonding on the *g*-tensor of pyrrolidine spin labels, such as MTSSL, was investigated by the restricted open-shell Hartree−Fock (ROHF) method.[12]

In our study, the calculated EPR parameters present the same trends as those seen in the experiments. The possibility to separate different contributions to the *A*-values, i.e., the influence of the dielectric constant (ϵ) of the continuous media from that of hydrogen bonded solvent molecules, is one advantage with the computational approach. The *g*-tensor calculated with DFT methods provided a better agreement with experiments compared with previous ROHF *g*-tensor calculations. From the analysis of both experimental and calculated results, an explanation to how the EPR parameters of MTSSL are influenced by its local environment is presented, acknowledging the different propensities of protic solvents to form hydrogen bonds to the oxygen of the nitroxide group. We believe that these results are useful for the interpretation of rigid-limit EPR data from spin-labeled proteins so that the observed parameter shifts can be "translated" into certain environmental properties.

2. Background

2.1. EPR Parameters. Interactions between the electron spin of free radicals and external magnetic fields are described by the spin Hamiltonian

$$H_{\text{spin}} = \mu_B \mathbf{SgB} + \mathbf{SAI} \tag{1}$$

The Zeeman term describes the interaction between the electron spin **S** and the external magnetic field **B**, parametrized by the *g*-tensor **g**. $\mu_B = e\hbar/2m_e$ is the Bohr magneton. The hyperfine interaction between **S** and the nuclear spin **I** is described by the *A*-tensor **A**. The *g*-tensor is calculated as a correction to the free electron value, $g_e = 2.002319$

$$\mathbf{g} = g_e\mathbf{1} + \Delta\mathbf{g} \tag{2}$$

The *g*-shift $\Delta\mathbf{g}$ consists of several terms derived from relativistic quantum mechanics,[27] of which the spin−orbit coupling (SOC) and orbital Zeeman (OZ) cross terms constitute the dominating parts. The SOC/OZ term is calculated from

$$\Delta g_{\text{SOC/OZ}} \propto \frac{\langle\Psi_0|H_{\text{SOC}}|\Psi_n\rangle\langle\Psi_n|H_{\text{OZ}}|\Psi_0\rangle}{E_0 - E_n} \tag{3}$$

where H_{SOC} and H_{OZ} are the Hamilton operators for each cross term, respectively, and $E_0 - E_n$ is the energy difference between the ground state $|\Psi_0\rangle$ and excited states $|\Psi_n\rangle$. A more detailed description of the different contributions to the *g*-shift is given in Malkina et al.[22]

The isotropic *g*-value is defined as

$$g_{\text{iso}} = \frac{g_{xx} + g_{yy} + g_{zz}}{3} \tag{4}$$

where g_{xx}, g_{yy}, and g_{zz} are the diagonal elements of **g**.

The hyperfine coupling *A*-tensor consists of two terms

$$\mathbf{A} = A_{\text{iso}}\mathbf{1} + \mathbf{A}_{\text{dip}} \tag{5}$$

The isotropic term A_{iso} (the Fermi contact term) is related to the spin density at the nucleus, i.e., the nitrogen in the present study, and is calculated from the Fermi contact Hamiltonian

$$H_{\text{iso}} = -\frac{2}{3}g_e\gamma_e\gamma_N\mu_0\delta(\mathbf{r}_N)\mathbf{S}\cdot\mathbf{I} \tag{6}$$

where γ_e and γ_N are the magnetogyric ratios for the electron and nucleus, respectively, μ_0 is the vacuum permeability, and $\delta(\mathbf{r}_N)$ is the delta function which extracts the spin density at the nucleus. $\mathbf{A}_{\text{dip}}$ in eq 5 corresponds to the classical dipolar coupling between magnetic dipoles and is calculated from the hyperfine interaction Hamiltonian

$$H_{\text{dip}} = \frac{g_e\gamma_e\gamma_N\mu_0}{4\pi}\left(\frac{\mathbf{S}\cdot\mathbf{I}}{r_N^3} - 3\frac{(\mathbf{S}\cdot\mathbf{r}_N)(\mathbf{r}_N\cdot\mathbf{I})}{r_N^5}\right) \tag{7}$$

where $\mathbf{r}_N$ is the electron-nucleus distance. In solvents with low viscosity (at ambient temperatures that is true for all solvents in this study), the fast rotational motion of the spin label causes $\mathbf{A}_{\text{dip}}$ to average out ($\mathbf{A}_{\text{dip}} = 0$).

2.2. Solvent Effects. In homogeneous solvents, the isotropic ^{14}N hyperfine coupling constant (A_{iso}) can be written as a sum of two terms

$$A_{\text{iso}} = A_{\text{iso}}^{\text{e}} + A_{\text{iso}}^{\text{h}} \tag{8}$$

where A_{iso}^{e} is the electrostatic interaction term and A_{iso}^{h} is the hydrogen bonding term.[4] Equation 8 assumes that there are no other specific interactions than hydrogen bonding. Comparisons with the Onsager reaction field model[28] show a linear relationship between A_{iso} and $(\epsilon - 1)/(\epsilon + 1)$ for nitroxide radicals in aprotic solvents ($A_{iso}^{h} = 0$) with dielectric constant ϵ.[4,29,30] That is, A_{iso} is higher in solvents with high ϵ than in solvents with low ϵ. This solvent effect can be understood as a perturbation of the electronic structure of the NO group. Polarity changes in the surrounding media induce shifts in the spin density; i.e., a more polar solvent causes an increased spin density on the nitrogen atom and thereby a stronger interaction between the free electron and the nitrogen nucleus, resulting in a higher A_{iso}. In protic solvents, A_{iso} is further increased ($A_{iso}^{h} > 0$).[3,4,30] Thus, A_{iso} is higher in protic solvents than in aprotic solvents with similar ϵ.[3,4,29,31,32] Due to the relation between **A** and A_{iso} (eq 5), similar trends are expected for A_{zz}.

The solvent dependence of the isotropic *g*-value (g_{iso}) was interpreted by Kawamura et al. according to Stone's theory.[3,33−35] The observed decrease in the *g*-value, as a result of increased polarity of the solvent or hydrogen bonding, was concluded to originate from decreased unpaired electron density on the oxygen and increased nπ* excitation energy.

3. Experimental Methods

3.1. Sample Preparation and Analysis. The spin label (1-oxyl-2,2,5,5-tetramethylpyrroline-3-methyl)methanethiosulfonate (MTSSL), obtained from Reanal (Budapest, Hungary), was dissolved in dimethyl sulfoxide (DMSO). Two stock solutions of MTSSL (100 mM) were prepared. In the first, a 10-fold excess of β-mercaptoethanol over MTSSL was added. The reaction was allowed to take place for several hours in the dark at room temperature. The second solution consisted of dissolved MTSSL alone. The MTSSL stock solutions were then added to various solvents, diluting MTSSL 100 times to a final MTSSL concentration of 1 mM. The solvents used were (ϵ-values taken from Weast,[36] $T = 20-25$ °C; "p" and "a" mean protic and aprotic): formamide $\epsilon = 109$ (p), water $\epsilon = 80.4$ (p) (10 vol % glycerol added to make it a better glass; its influence on the resulting ϵ is neglected), ethyleneglycol $\epsilon = 38.7$ (p), methanol $\epsilon = 33.6$ (p), ethanol $\epsilon = 24.3$ (p), acetone $\epsilon = 20.7$ (a), 1-propanol $\epsilon = 20.1$ (p), 1-butanol $\epsilon = 17.8$ (p), 1-hexanol $\epsilon = 13.3$ (p), pyridine $\epsilon = 12.3$ (a), 1-heptanol $\epsilon = 11.1$ (p), 1-octanol $\epsilon = 10.3$ (p), 1-nonanol $\epsilon \approx 9$ (p), methyl formate $\epsilon = 8.5$ (a), 1-decanol $\epsilon = 8.1$ (p), ethyl acetate $\epsilon = 6.0$ (a), and toluene $\epsilon = 2.4$ (a). Note that not all solvents were used in every set of experiments.

The two stock solutions were analyzed with GC-MS (gas chromatography with mass spectrometric detection) on an HP 6890 GC-HP 5973 mass selective detector (Hewlett-Packard, Palo Alto, CA). Capillary column: HP-5 MS, 30 m × 0.25 mm, phase 0.25 μm; carrier gas, He, 40 cm/s; temperature program 100 °C for 3 min (MTSSL) or 10 min (MTSSL + β-mercaptoethanol), 10 °C/min, 300 °C (5 min), split injection, 1.5 μL, split ratio 50:1.2; scan range 12−400 u. Methylene chloride was used to dissolve MTSSL, as DMSO is not suitable for GC experiments. The MTSSL concentration was 0.5 mg/mL (2 mM). A 10-fold excess of β-mercaptoethanol was used.

3.2. X-Band EPR Experiments. 9-GHz EPR measurements were carried out using a Bruker CW X-band spectrometer consisting of a combination of the ER200D-SRC and ESP300 systems. A 4102 ST resonator connected to the 200 mW microwave bridge was used. Measurements of MTSSL and MTSSL−β-mercaptoethanol in various solvents were performed in the liquid state at room temperature (21 °C) and in the rigid state (77 K).

Liquid State. The samples were transferred into 1-mm quartz capillary tubes (Wilmad Glass, Buena, NJ), ∼40 μL sample volume/tube. Measurements were performed at 1 mW microwave power using a modulation frequency of 100 kHz with an amplitude of 1.0 G and the measurement time was 105 s. The frequency drift during each measurement was less than 0.000005 GHz. The magnetic field was calibrated before and after the solvent measurements using a LiTCNQ EPR standard ($g_{iso} = 2.002675 \pm 0.000001$). All samples were measured at 2−4 independent occasions.

Rigid State. The samples were transferred into 4-mm quartz capillary tubes (Wilmad Glass), ∼200 μL sample volume/tube, followed by two freeze−evacuate−thaw cycles before a final freeze-evacuation ($p < 10^{-4}$ mbar) event to reduce the amount of oxygen dissolved in the sample. Measurements were made at 77 K using a standard EPR liquid nitrogen dewar (Wilmad Glass) at 0.1 mW microwave power and a modulation frequency of 100 kHz with an amplitude of 3 G. The measurement time was 14 min. The samples were studied at two separate occasions.

3.3. W-Band EPR Experiments. High-frequency (95 GHz) EPR measurements were performed with a Bruker Elexsys 680 FT/CW spectrometer with an Oxford 5.8 T split coil magnet. The system uses two separate oscillators. The stabilized frequency of the Gunn oscillator was measured to be 84.499844 GHz, and it is added to the second Gunn oscillator operating at 9−10 GHz. The magnetic field was calibrated using a Mn^{2+}/CaO EPR standard. The samples with MTSSL−β-mercaptoethanol in different solvents were introduced in quartz capillary tubes, $\phi_o = 0.9$ mm (Wilmad Glass), ∼2 μL sample volume/tube. To achieve a stable sample temperature, a standard helium flow system was connected to the Oxford CF 935 helium cryostat. Samples were frozen by inserting them into the precooled cryostat. All rigid-limit spectra were recorded at 40 K to restrict the molecular motion of the spin label. At this temperature, the samples adopt a frozen glassy state. To avoid hysteresis effects of the superconducting magnet, single-scan experiments were made. A modulation frequency of 100 kHz was used with an amplitude sufficiently low to avoid distortion of the line shape ($A_{mod} \leq {}^{1}/_{5}$ of the peak-to-peak line width of the central line). Low microwave powers (45−55 dB attenuation) were used to avoid line shape distortions due to contribution from the dispersion signal often perturbing W-band EPR spectra. In this way, spectra with well-defined powder patterns were obtained. Due to the complexity of W-band measurements, only one series of solvent measurements was performed.

3.4. EPR Data Analysis. Analysis of isotropic and rigid-limit X-band spectra were carried out using the WINEPR 1.22 software (Bruker Analytik GmbH, Rheinstetten/Karlsruhe, Germany). Spectra were baseline corrected, and the isotropic parameters A_{iso} and g_{iso}, as well as the anisotropic A_{zz}, were read directly from the spectra (Figure 2a,b). The error in the A_{zz} read-off was estimated to be ±0.12 G (±1 data point), whereas the errors in A_{iso} and g_{iso} were expected to be $<\pm 0.10$ G and $<\pm 0.00006$, respectively (determined from the intersections with the field axis through linear interpolation of the two closest data points). Isotropic *g*-values were corrected according to the EPR standard and the difference in microwave frequency between sample and reference. The mean value of all parameters was determined as well as the standard deviation.

Rigid-limit W-band spectra were baseline corrected, scaled, and then simulated using the WINEPR SimFonia 1.25 software (Bruker Analytik GmbH). First-order perturbation theory was

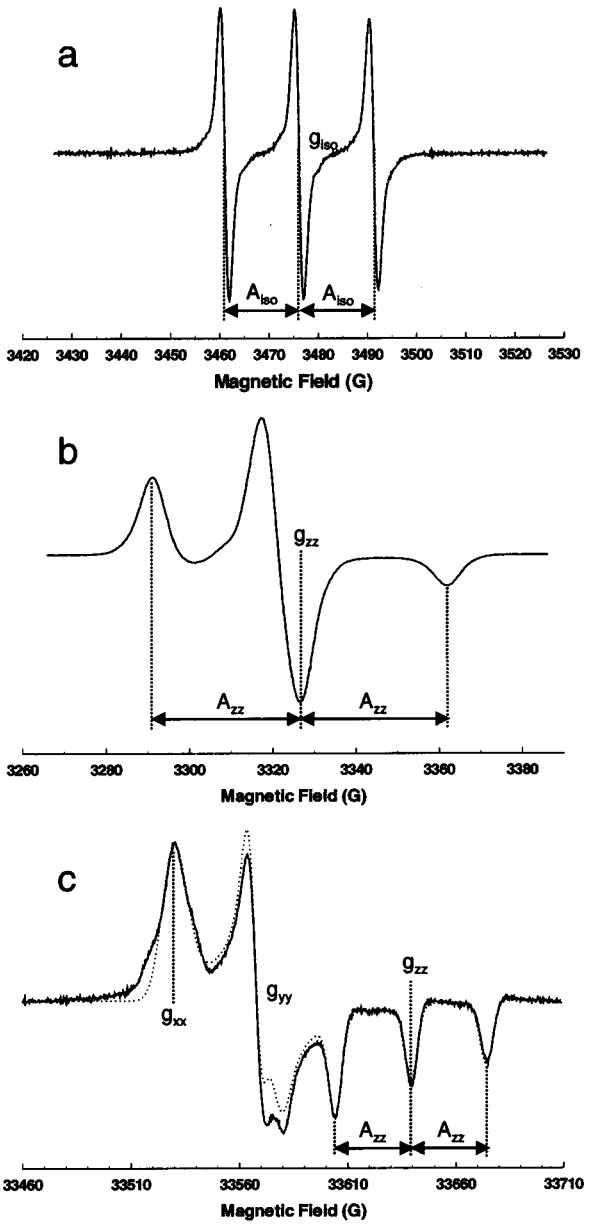

Figure 2. Definition of EPR parameters of interest: (a) Isotropic *g*- and *A*-values (g_{iso}, A_{iso}) obtained from isotropic solution spectra at X-band. (b) The *z*-component of the *g*- and *A*-tensors (g_{zz}, A_{zz}) is resolved in rigid-limit spectra at X-band. (c) The components of the *g*- and *A*-tensors, [g_{xx}, g_{yy}, g_{zz}] and [A_{xx}, A_{yy}, A_{zz}], are obtained from simulations of rigid-limit spectra at W-band.

selected for the calculation of the hyperfine splittings. The number of θ and ϕ angles in the powder average were 200 and 50, respectively. Purely Gaussian line shapes were used. From the simulations the principal components of the *g*-tensor [g_{xx}, g_{yy}, g_{zz}] and *A*-tensor [A_{xx}, A_{yy}, A_{zz}] were obtained (Figure 2c). However, A_{xx} and A_{yy} are not resolved in spectra even at W-band. In comparison, the lower resolution at X-band only admits the g_{zz} and A_{zz} components to be read directly from rigid-limit spectra (Figure 2b). The *g*-tensor components were corrected according to the Mn^{2+}/CaO standard.

W-band EPR spectra of several solvents contained a second species, which had a larger g_{xx} value than that of the majority species. The solvents in which the component was observed were 1-octanol, 1-hexanol, pyridine, ethanol, 1-butanol, and methanol. The contribution of the second component was approximately 1:1 (higher g_{xx}:lower g_{xx}) for the first four solvents and 1:3 and 1:6 for the last two, respectively. The value of g_{xx} = 2.00874 was independent of the solvent. Besides the g_{xx} component, no further splittings were resolved in the spectra. Errors in the *g*- and *A*-tensor components were estimated from the sensitivity of the simulations to the fitting parameters. Larger errors for some samples result from poor signal-to-noise of the data or, in other cases, from deviations of the line shape from the expected powder distribution, which is probably largely due to residual dispersive contributions in the W-band EPR spectra. This error only refers to the relative magnitude of the individual components g_{ii} with respect to each other. An absolute *g*-value calibration was not attempted.

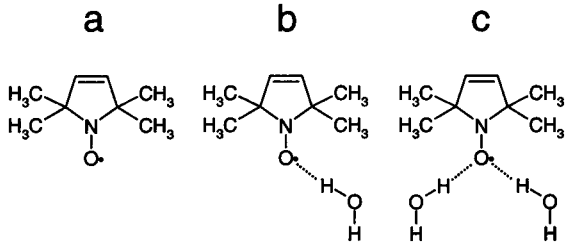

Figure 3. Spin label (MSL) and water molecules to model hydrogen bonding: (a) model A, no H-bonds; (b) model B, one H-bond; and (c) model C, two H-bonds.

To facilitate comparison of experimental and calculated data, the isotropic and anisotropic *A*-values are presented as relative values. Toluene was chosen as reference, since it has the lowest dielectric constant of the solvents used and is aprotic. Thus, experimental relative *A*-values are defined as

$$\Delta A_{iso} = A_{iso}(\text{solvent}) - A_{iso}(\text{toluene}) \quad (9a)$$

$$\Delta A_{zz} = A_{zz}(\text{solvent}) - A_{zz}(\text{toluene}) \quad (9b)$$

and relative *A*-values from calculated data are defined as

$$\Delta A_{iso}^{A,B,C} = A_{iso}^{A,B,C}(\epsilon) - A_{iso}^{A}(\epsilon=2.4) \quad (9c)$$

$$\Delta A_{zz}^{A,B,C} = A_{zz}^{A,B,C}(\epsilon) - A_{zz}^{A}(\epsilon=2.4) \quad (9d)$$

where the letters in superscript correspond to the MSL models (Figure 3). Experimental and calculated *g*-values are presented as absolute values since the ϵ-dependence of the *g*-values could not be considered in the calculations.

4. Computational Methods

The MTSSL spin label consists of three parts: the nitroxide group, the pyrrolidine group with its methyl groups, and the linker with a chemically active group that promotes covalent binding to a sulfur atom (Figure 1). Almost all unpaired electron density is localized on the nitroxide group of the spin label. In this study, MTSSL is also anchored to β-mercaptoethanol creating a stable complex. Variations in the linker structure was found to have only minor influence on the spin density distribution of the radical.[12] Thus, in the calculations of EPR parameters, it was sufficient to use the truncated MSL as a model of the two MTSSL variants. The geometric structures for MSL with/without hydrogen bonded solvent molecules (Figure 3) were optimized with the B3LYP/6-31G** method using the Gaussian98 program.[37] The *A*-tensor was calculated with the B3LYP/EPR-II method also implemented in Gaussian98. The *g*-tensor was calculated with the BP86/IGLO-II method using the deMon program.[22,38] The (5,2;5,2) auxiliary basis was chosen for carbon, nitrogen, and oxygen atoms, and (5,1;5,1) for hydrogens. In the *g*-tensor calculations, the gauge origin problem was tackled with the individual gauge for localized orbitals

(IGLO) method[39] using the Pipek−Mezey (PM) algorithm[40] for localizing the orbitals. The orbitals corresponding to the 1s orbitals of the heavy atoms were localized separately from all the valence orbitals. The full one- and two-electron spin−orbit operator was approximated by an effective one-electron/one-center operator[41] using the atomic mean-field (AMFI) software.[42]

Contributions to the *g*- and *A*-tensors of the MSL model due to the influence of the solvent were defined and calculated in two separate ways:

(1) The self-consistent reaction field (SCRF) polarizable continuum model (PCM) was used to estimate solvent effects on the *A*-tensor. In this model, the solvent is considered as a uniform medium with dielectric constant ϵ. MSL was, according to the PCM model, inserted in a cavity formed from the van der Waals surface of the radical. The solvation free energy for this system can be written as

$$\Delta G_{\text{solvation}} = \Delta G_{\text{cavity}} + \Delta G_{\text{dispersion}} + \Delta G_{\text{electrostatic}} \quad (10)$$

where ΔG_{cavity} is the energy cost of creating the cavity and $\Delta G_{\text{dispersion}}$ is approximately the van der Waals energy between MSL and the solvent. The charge distribution of MSL polarizes the medium, and the polarized medium influences the molecule giving rise to $\Delta G_{\text{electrostatic}}$.

(2) Zero to two solvent molecules were defined to form hydrogen bonds to the nitroxide oxygen of MSL. We have previously shown that the number of hydrogen bonds influences the EPR parameters of MSL, whereas the kind of hydrogen-bonding solvent molecule is less important.[12] Therefore, water molecules were used in all calculations to model hydrogen bonds. This approach gives us three separate structure models of the interaction between MSL and its microenvironment (Figure 3).

5. Results

5.1. Sample Analysis. The composition of the MTSSL stock solutions was determined from chromatograms recorded in the GC-MS experiments (data not shown). The most intense peak of the mass spectrum of MTSSL, at a retention time of 14.8 min, was observed at *m*/*z* 264, i.e., the molecular mass of MTSSL. No compound corresponding to dimerized MTSSL (2 × 185=370 u) was detected. When a mixture of MTSSL and β-mercaptoethanol was analyzed, the mass spectrum of the most intense peak, at 13.3 min, showed a line at *m*/*z* 262. No peak was found corresponding to free MTSSL (264 u). Thus, all MTSSL was exclusively covalently bound to β-mercaptoethanol.

5.2. Solvent Effects on the Nitrogen Hyperfine Coupling. The isotropic hyperfine coupling constants (A_{iso}) determined for MTSSL and MTSSL−β-mercaptoethanol (from now on abbreviated MTSSL-β) in different solvents are presented in Figure 4a as a function of ϵ. The magnitude of A_{iso} was read-off from the X-band spectra, of which one example is shown in Figure 2a. The dominant trend is that A_{iso} increases nonlinearly with increasing ϵ of the solvent. We also observed an almost constant shift in A_{iso} to slightly higher values when MTSSL-β was used instead of MTSSL. A_{iso}-values were calculated by the DFT method for MSL as a function of ϵ for models A−C (Figure 3). The calculated A_{iso}-values differed in absolute magnitude from the experimental values; therefore, relative A_{iso}-values (ΔA_{iso}) were used for comparison with toluene as reference solvent (eq 9a,c). In Figure 4b, the experimental ΔA_{iso}-values of MTSSL are displayed as a function of ϵ. Extreme values for ΔA_{iso} were found for MTSSL in toluene on the one end and water on the other, spanning a range of ∼1.8 G. Among the alcohols, the spread in ΔA_{iso} is much smaller (∼0.1 G from ethanol to 1-decanol). ΔA_{iso}-values from the DFT calculations are shown as lines in Figure 4b. For model A (solid line), $\Delta A_{\text{iso}}{}^{A}$ increases sharply for media with ϵ-values up to about 10, whereas further increase in ϵ causes a relatively small response of $\Delta A_{\text{iso}}{}^{A}$. At $\epsilon > 30$, $\Delta A_{\text{iso}}{}^{A}$ was close to constant. The ϵ-dependence of model B and C show the same behavior, but they are shifted to higher values of ΔA_{iso} due to the influence of one or two hydrogen bonds. Moreover, two hydrogen bonds to the spin label cause a 3−8 times larger increase in ΔA_{iso} compared with one hydrogen bond (this effect is enhanced for high ϵ-values). Comparing experimental and calculated ΔA_{iso}-

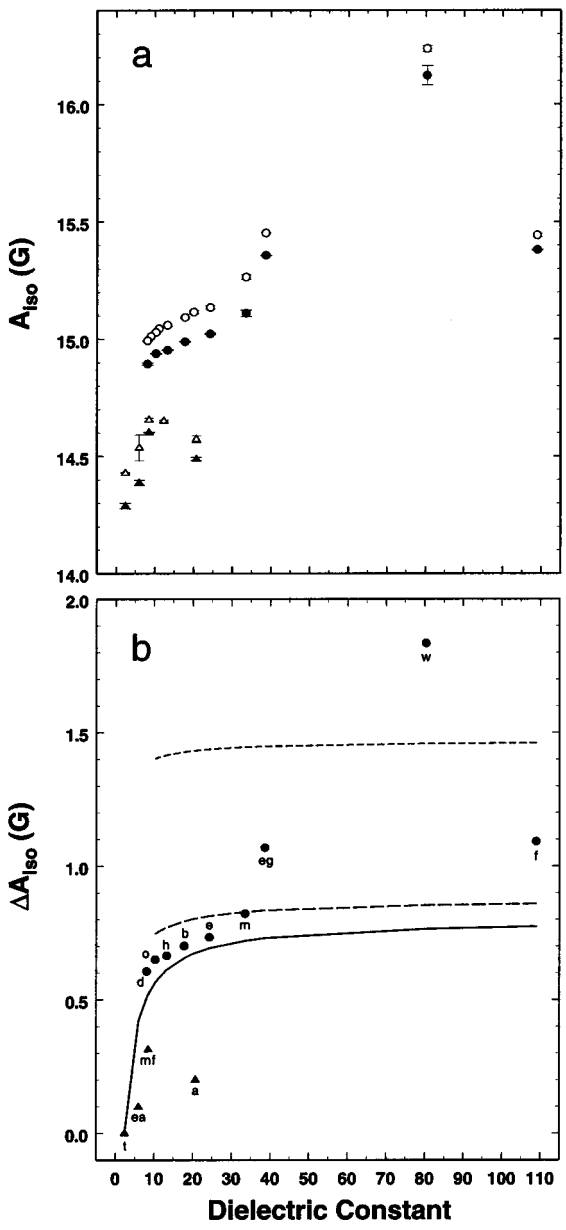

Figure 4. Solvent dependence of the isotropic hyperfine coupling constant, A_{iso}. (a) Experimental A_{iso}-values obtained from solution X-band experiments of (●,▲) MTSSL and (○,△) MTSSL−β-mercaptoethanol in different solvents (circle = protic solvent, triangle = aprotic solvent). (b) Experimental ΔA_{iso}-values (eq 9a) determined from MTSSL data in panel a. DFT calculated ΔA_{iso}-values (eq 9c) represent the three models described in Figure 3: (—) model A; (— —) model B; (- - -) model C. Lower-case letters are abbreviations of the different solvents (*t* = toluene, ea = ethyl acetate, *d* = 1-decanol, mf = methyl formate, o = 1-octanol, h = 1-hexanol, b = 1-butanol, a = acetone, e = ethanol, m = methanol, eg = ethyleneglycol, w = water, and f = formamide).

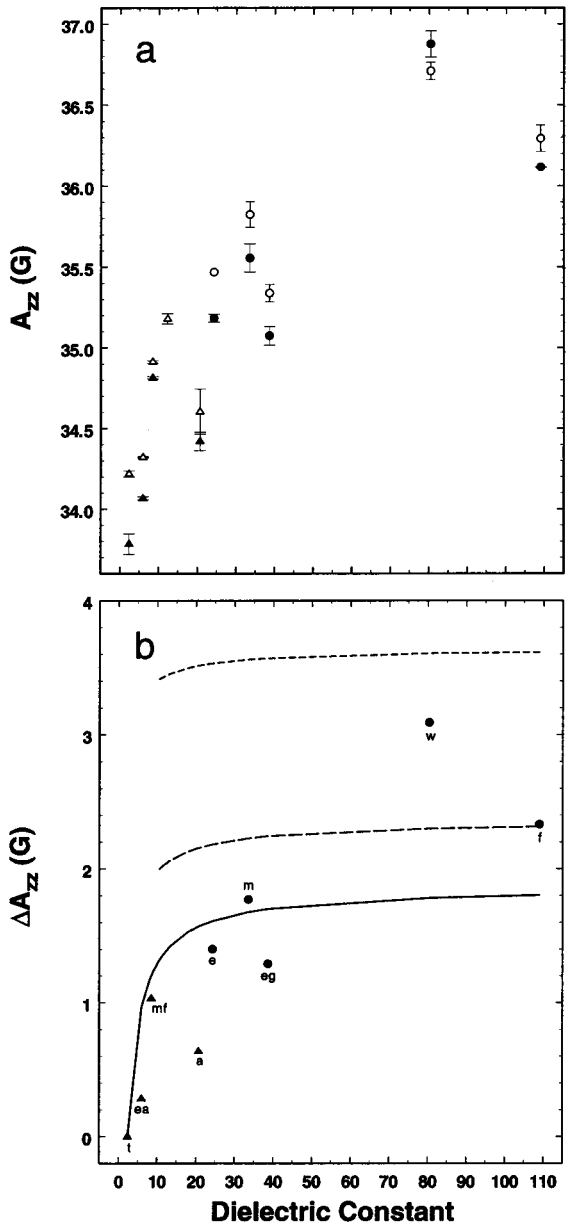

Figure 5. Solvent dependence of the *z*-component of the anisotropic hyperfine coupling tensor, A_{zz}. (a) Experimental A_{zz}-values obtained from rigid-limit X-band experiments of (●,▲) MTSSL and (○,△) MTSSL−β-mercaptoethanol in different solvents (circle = protic solvent, triangle = aprotic solvent). (b) Experimental ΔA_{zz}-values (eq 9b) determined from MTSSL data in panel a. DFT calculated ΔA_{zz}-values (eq 9d): (—) model A; (— —) model B; (- - -) model C. Solvent abbreviations are as defined in Figure caption 4b.

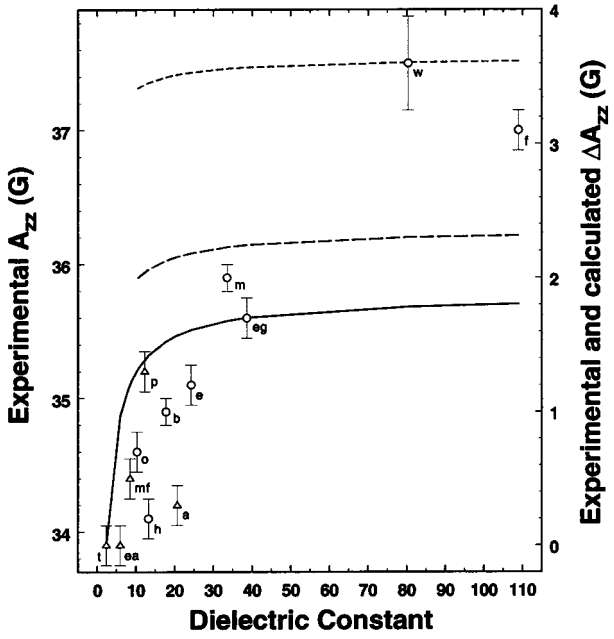

Figure 6. Solvent dependence of A_{zz} monitored by high-field EPR. Experimental A_{zz}-values are obtained from rigid-limit W-band experiments of MTSSL−β-mercaptoethanol in different solvents (○ = protic, △ = aprotic). Experimental and calculated ΔA_{zz}-values are given (eq 9b,d) on the right axis. The DFT calculated ΔA_{zz}-values according to (—) model A; (— —) model B; (- - -) model C are the same as those in Figure 5b. Solvent abbreviations are as defined in Figure caption 4b, except p = pyridine.

data will allow to determine the degree of hydrogen bonding in the different solvents, as described in section 6.1.

The anisotropic hyperfine parameters, in particular the *z*-component of the anisotropic hyperfine coupling tensor (A_{zz}) was obtained from measurements of MTSSL and MTSSL-β in frozen solutions. It was measured directly from the rigid-limit X-band spectra, as shown in Figure 2b. Figure 5a presents these data as a function of ϵ. Similarly to A_{iso}, A_{zz} follows an increasing trend when ϵ is increased, but the values are considerably more scattered compared to the isotropic values. The standard deviation in A_{zz} for multiple measurements on individual solvents is also larger than for A_{iso}. Data from the longer alcohols (1-decanol to 1-butanol) are not included in the plot because repetitive measurements showed that A_{zz}-values were not reproducible, either with MTSSL or MTSSL-β. The data from the alcohols in this rather narrow ϵ-region ($\epsilon = 8.1-17.8$) were highly scattered ($A_{zz} = 34-36$ G), without any obvious correlation with A_{iso} as seen in Figure 4a. The most likely reason for this behavior is induced inhomogeneities in the samples upon freezing to 77 K. As for the isotropic values, the A_{zz}-values of MTSSL-β were somewhat higher than those of MTSSL (water being the only exception). The experimental A_{zz}-values of MTSSL are compared with DFT-calculated ΔA_{zz}-values (eq 9b,d) in Figure 5b. ΔA_{zz} from experiments spanned over a range of about 3 G, i.e., >60% larger compared with ΔA_{iso}. Larger variations in ΔA_{zz} were also obtained from the calculations, as a result of the redistribution of spin density from oxygen to nitrogen due to the increasing ϵ ($\Delta A_{zz}^{A,\epsilon=109} = 1.8$ G, whereas $\Delta A_{iso}^{A,\epsilon=109} = 0.8$ G) and hydrogen bonding ($\Delta A_{zz}^{C,\epsilon=109} - \Delta A_{zz}^{A,\epsilon=109} = 1.8$ G, whereas $\Delta A_{iso}^{C,\epsilon=109} - \Delta A_{iso}^{A,\epsilon=109} = 0.7$ G). The increase in ΔA_{zz} due to two hydrogen bonds was 2−3 times larger than that due to one hydrogen bond. This differs from the calculated values for ΔA_{iso}, where the addition of the second hydrogen bond causes a significantly larger increase in ΔA_{iso} (compare Figures 4b and 5b). The experimental ΔA_{zz}-values are distributed rather differently in relation to the curves of models A−C compared to the isotropic values; however, the general trend is similar.

Rigid-limit W-band EPR experiments were performed on MTSSL-β, resulting in significantly increased spectral resolution compared to X-band spectra, as can be seen in Figure 2c, where a representative spectrum is shown. Experimental A_{zz}-values are presented in Figure 6, together with values calculated by the DFT method (models A−C) as a function of ϵ. Data of the longer alcohol chains are included, although it is likely that their A_{zz}-values depend on freezing conditions as discussed for the X-band experiments. Going to high-field EPR did not change the overall trend of ΔA_{zz} when changing the properties of the solvent. Some differences are observed between the A_{zz}-

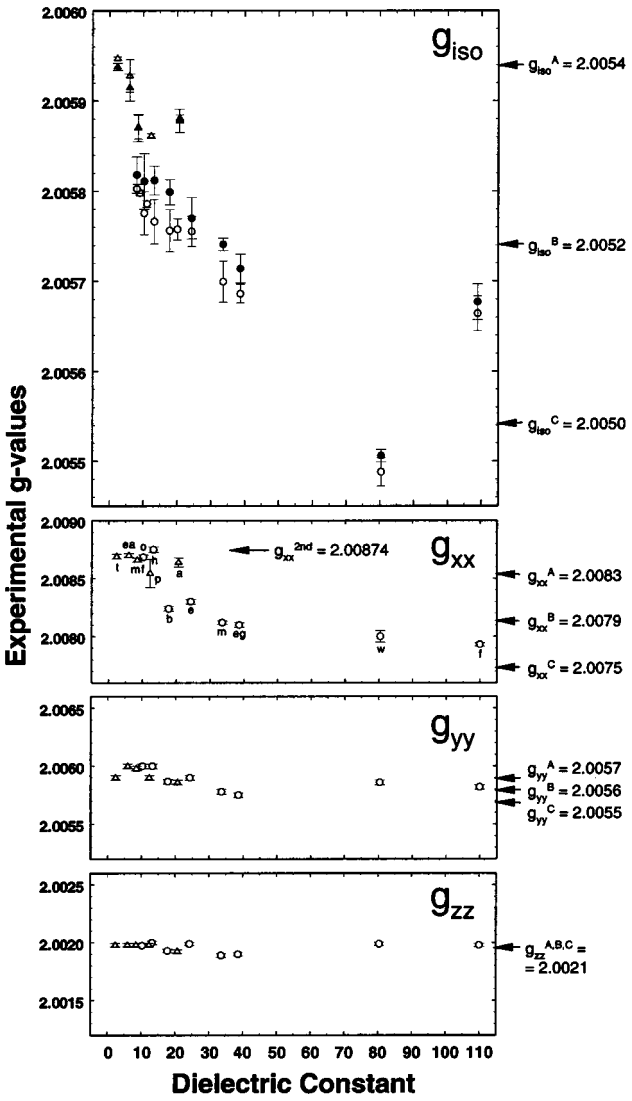

Figure 7. Solvent dependence of the isotropic *g*-value and the anisotropic *g*-tensor components. Experimental g_{iso}-values are obtained from solution X-band experiments of (●,▲) MTSSL and (○,△) MTSSL−*β*-mercaptoethanol in different solvents (circle = protic solvent, triangle = aprotic solvent). g_{xx}-, g_{yy}- and g_{zz}-values are obtained from rigid-limit W-band experiments using (○,△) MTSSL−*β*-mercaptoethanol in different solvents. DFT calculated *g*-values, given in the right part of the figure, correspond to models A−C (Figure 3), where MSL is assumed to be in a vacuum. Calculated data are not in quantitative agreement with the vertical axis, but are scaled in the same way. Note that the range of the g_{iso} plot is much smaller compared to the ranges of the other three plots. Solvent abbreviations are as defined in Figure captions 4b and 6.

parameters obtained at W-band and X-band (cf. Figures 5a and 6). Whether this is due to the difference in measuring temperature (40 K at W-band compared to 77 K at X-band) or other factors cannot be decided at present. One indication of sample heterogeneity is the spectral signature of a second species observed in these solvents (see section 3.4).

5.3. Solvent Effects on the *g*-Values. The isotropic *g*-value (g_{iso}) as a function of ϵ of the solvent, determined from X-band solution spectra of MTSSL and MTSSL-*β*, is shown in Figure 7. The principal components of the anisotropic *g*-tensor ([g_{xx}, g_{yy}, g_{zz}]) obtained from the W-band EPR rigid-limit spectra of MTSSL-*β* in different solvents are also shown. The *g*-tensor component along the NO bond (g_{xx}) is most sensitive to changes in the properties of the solvent. The overall trend observed is that g_{iso} and g_{xx} decrease as the polarity of the solvent is

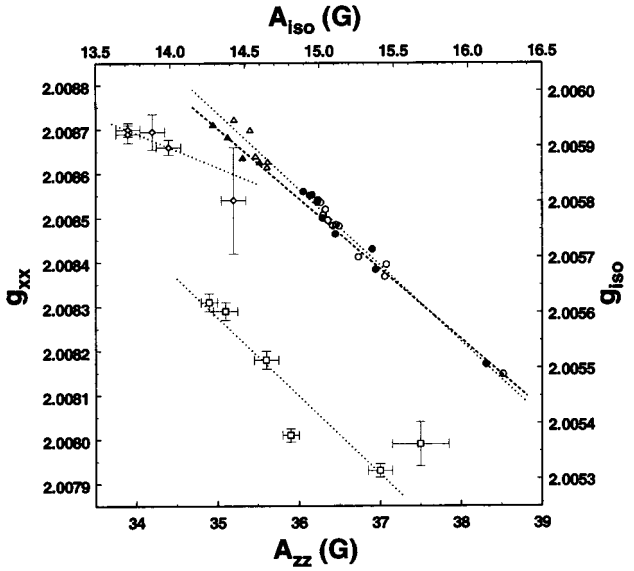

Figure 8. Correlation between the EPR parameters that are most sensitive to changes in the environment of the spin label. Correlation between g_{iso} and A_{iso} for (●, ▲) MTSSL and (○,△) MTSSL−*β*-mercaptoethanol, as well as between g_{xx} and A_{zz} for (□, ◇) MTSSL−*β*-mercaptoethanol. Symbol notations: circle, square = protic; triangle, diamond = aprotic. The dotted lines correspond to linear regressions of the data sets ($R_{●▲}$ = 0.983, $R_{○△}$ = 0.986, $R_{□}$ = 0.926, $R_{◇}$ = 0.907). Values for 1-hexanol and 1-octanol were excluded from this figure because the second species (for details, see text) causes a large error in g_{xx}. The g_{xx}-values are calibrated relative to g_{zz}.

increased. The determination of g_{xx} for the longer chain alcohols (for details, see section 3.4) was hampered by the occurrence of a second spectral component with a larger g_{xx}-value (Figure 2c), g_{xx} = 2.00874, which was independent of the solvent (represented with a horizontal arrow in Figure 7). Thus, for solvents with smaller g_{xx}-values, the second component was well resolved. For solvents with larger g_{xx}, such as 1-octanol and 1-hexanol, the second component was not resolved making the analysis of g_{xx} in these solvents more uncertain. A small dependence of g_{iso} on the structure of the linker was seen for most of the solvents. Furthermore, for the protic solvents g_{iso}-values were generally smaller than those for the aprotic solvents of comparable ϵ. The larger uncertainties in g_{iso} compared to A_{iso} were expected since g_{iso} is directly influenced by shifts in the magnetic field and uncertainties in the *g*-value calibration. Despite these errors, however, the shifts in g_{iso} are large enough to establish a solvent dependence. In analogy to the treatment of Kawamura et al., g_{iso} is plotted against A_{iso}^3 and the W-band EPR parameters g_{xx} against A_{zz} (Figure 8). The lines indicate linear correlations between groups of solvents which will be discussed below.

The *g*-tensor components were calculated using DFT methods, assuming the three models illustrated in Figure 3. Calculated *g*-values are presented in Figure 7 as horizontal arrows to illustrate the decrease in the *g*-values due to one or two hydrogen bonds. As for the calculated hyperfine coupling constants, a quantitative agreement with experimental values was not achieved. To compare experimental and calculated results, the *g*-values of model B are positioned with guidance from the isotropic data (Figure 4b), i.e., at the values of methanol. According to calculated data, g_{xx} is most sensitive to changes in hydrogen bonding, followed by g_{yy} (4 times less sensitive), whereas g_{zz} is essentially constant at this accuracy. In contrast to the hyperfine coupling constants, each hydrogen bond reduces the *g*-values by the same amount.

TABLE 1: Experimental Isotropic and Anisotropic EPR Parameters of MTSSL in Some Solvents with Different Properties

solvent	ϵ[a]	g_{iso}[b] (Δg_{iso})	g_{xx}[c] (Δg_{xx})	g_{yy}[c] (Δg_{yy})	g_{zz}[c] (Δg_{zz})	A_{iso}[d] (ΔA_{iso})	A_{zz}[e] (ΔA_{zz})	A_{zz}[f] (ΔA_{zz})
toluene	2.4	2.00594	2.00869	2.00590	2.00198	14.29	33.78	33.9
ethanol	24.3	2.00577	2.00830	2.00590	2.00199	15.02	35.18	35.1
		(−0.00017)	(−0.00039)	(−0.00000)	(0.00001)	(0.73)	(1.40)	(1.2)
methanol	33.6	2.00574	2.00812	2.00578	2.00189	15.11	35.56	35.9
		(−0.00020)	(−0.00057)	(−0.00012)	(−0.00009)	(0.82)	(1.78)	(2.0)
water	80.4	2.00551	2.00800	2.00586	2.00199	16.12	36.88	37.5
		(−0.00043)	(−0.00069)	(−0.00004)	(0.00001)	(1.83)	(3.10)	(3.6)

[a] ϵ of solvent at 20−25 °C.[36] The ϵ of water is used to describe the water/glycerol mixture; i.e., the influence from the 10% glycerol on the resulting ϵ is neglected. [b] $\Delta g_{iso} = g_{iso}$(solvent) − g_{iso}(toluene). [c] $\Delta g_{ii} = g_{ii}$(solvent) − g_{ii}(toluene), where *ii* represents the different *g*-components. [d] ΔA_{iso} is determined according to eq 9a. Both parameters are reported in Gauss. [e] X-band data. ΔA_{zz} is determined according to eq 9b. Both parameters are reported in Gauss. [f] W-band data obtained from MTSSL-β. ΔA_{zz} is determined according to eq 9b. The parameters are reported in Gauss.

TABLE 2: Calculated Isotropic and Anisotropic EPR Parameters of the MSL Spin Label Model in Some Media with Different Properties

medium	ϵ[a]	model[b]	g_{iso}[c] (Δg_{iso})	g_{xx}[c] (Δg_{xx})	g_{yy}[c] (Δg_{yy})	g_{zz}[c] (Δg_{zz})	A_{iso}[d] (ΔA_{iso})	A_{zz}[e] (ΔA_{zz})
toluene	2.4	A	2.00538	2.00832	2.00568	2.00214	9.80	28.79
ethanol	24.3	A	2.00538	2.00832	2.00568	2.00214	10.49	30.40
			(0.00000)	(0.00000)	(0.00000)	(0.00000)	(0.69)	(1.61)
methanol	33.6	B	2.00521	2.00788	2.00561	2.00214	10.62	31.02
			(−0.00017)	(−0.00044)	(−0.00007)	(0.00000)	(0.82)	(2.23)
water	80.4	C	2.00506	2.00750	2.00554	2.00213	11.25	32.40
			(−0.00032)	(−0.00082)	(−0.00014)	(−0.00001)	(1.45)	(3.61)

[a] ϵ of medium at 20−25 °C.[36] [b] Applied structural model of the interaction between spin label and molecules of the medium according to Figure 3. The given model for each medium corresponds to the situation with closest resemblance to the respective medium. [c] *g*-values are determined for MSL in a vacuum; thus, only differences in hydrogen bonding are considered. $\Delta g_{ii} = g_{ii}^{A,B,C} - g_{ii}^{A}$, where *ii* represents the different *g*-components. [d] ΔA_{iso} is determined according to eq 9c. Both parameters are reported in Gauss. [e] ΔA_{zz} is determined according to eq 9d. Both parameters are reported in Gauss.

6. Discussion

In the present study, the hyperfine couplings of the nitrogen (A_{iso} and A_{zz}) and the *g*-values (g_{iso} and g_{xx}) of the spin label MTSSL were applied as indicators of local polarity and proticity. The main objectives were to study the response of MTSSL to various solvent environments and to make a quantitative analysis of the influence of the dielectric and hydrogen bonding properties of the medium on the EPR parameters. We investigated MTSSL in two forms: as a neat molecule (MTSSL) and in a β-mercaptoethanol linked form (MTSSL-β) to test the impact of a modified linker segment of MTSSL. Both protic and aprotic solvents were chosen within a broad ϵ-range.

6.1. Nitrogen Hyperfine Couplings: A_{iso} and A_{zz}. From Figure 4, it can be concluded that A_{iso} is sensitive to the ϵ of the solvent and that A_{iso} increases monotonically, though not linearly with ϵ. This is in agreement with previous findings of nitroxide radicals.[3,4,29] In Table 1, A_{iso}- and ΔA_{iso}-values are summarized for MTSSL in some selected solvents, toluene, ethanol, methanol, and water. The absolute A_{iso}-values for the di-*tert*-butyl nitroxide radical (DTBNO) in these four solvents by Reddoch and Konishi are of quite different magnitude compared to those of MTSSL due to the major structural differences,[29] but the ΔA_{iso}-values relative to toluene are very similar (ethanol: 0.69 G, methanol: 0.82 G, water: 1.78 G; cf. Table 1). Thus, the shift in A_{iso} due to changed environmental properties seems rather conserved despite the structural variation of the spin label.

In the following, the experimental A_{iso}-values are compared to the results of DFT calculations. Some of our calculated results are presented in Table 2. The agreement between experimental and calculated absolute A_{iso}-values (Tables 1 and 2) is poor (~40% larger experimental values). This is attributed to the fact that A_{iso} is determined by the spin density in the s-orbital of the nitrogen (Fermi contact interaction) and the difficulty in creating a basis set that accurately describes this spin density. We therefore compare the experimental and calculated hyperfine coupling constants with reference to toluene (ΔA_{iso}). Since toluene is both aprotic and the most apolar of the solvents used in this study, the change in A_{iso} can separately be interpreted in terms of the dielectric properties of the environment and the degree of hydrogen bonding.

In Figure 4b, the measured ΔA_{iso}-values are compared to DFT calculations. For MTSSL in most of the protic alcohols, 1-decanol to ethanol, a smooth dependence of ΔA_{iso} on the ϵ-value is seen, which resembles the curves from the DFT calculations for no or one hydrogen bond, suggesting that less than one hydrogen bond is formed on average, independent of the length of the carbon chain. ΔA_{iso} for MTSSL in two of the aprotic solvents (methyl formate and ethyl acetate) reasonably agrees with the result of the DFT calculations for the model without hydrogen bonds, whereas ΔA_{iso} for MTSSL in acetone is significantly lower than what would be expected from its tabulated ϵ. In the more polar, protic solvents (methanol, ethyleneglycol, water, and formamide) MTSSL gives, to various extent, higher ΔA_{iso}-values than those anticipated from the ϵ of the solvents. The higher ΔA_{iso}-values might be explained by either a larger number of hydrogen bonds formed in these solvents at similar bond strengths, or higher bond strengths compared to the longer alcohols, since the influence of the ϵ-value on ΔA_{iso} was small in this region. Symons and Pena-Nuñes favor the former situation in the case of methanol and water, since a great difference in the strength of the hydrogen bonds are not expected.[43] Thus, the ΔA_{iso}-value for MTSSL in methanol may indicate a higher propensity to form hydrogen bonds than for example ethanol, and the resemblance to the calculated value of model B at the ϵ of methanol suggests that one hydrogen bond is formed on average. This result is in reasonable agreement with data reported in the literature. For example, Yagi and co-workers calculated the average number of hydrogen bonded methanol molecules to the $(CH_3)_2NO$

radical to be 0.33,[31,32] whereas Symons and Pena-Nuñes experimentally found it to be one on average to the DTBNO radical.[43] ΔA_{iso} for MTSSL in ethyleneglycol is between the curves calculated for one and two hydrogen bonds (Figure 4b). MTSSL in water results in a ΔA_{iso}-value larger than the value calculated for two hydrogen bonds. This fairly agrees with the previous findings of 1.33[31,32] and two[43] hydrogen bonds formed in water. For MTSSL in formamide, ΔA_{iso} is smaller than in water, despite the larger ϵ. Without calculating the effect of a nitrogen hydrogen bond donor, we cannot determine if this is due to weaker hydrogen bonds or a lower hydrogen bond donation propensity of the nitrogen in formamide compared to the oxygen in water. This comparison shows an overall good agreement between experimental and calculated ΔA_{iso}-values and allows the determination of relative degrees of hydrogen bonding. More uncertainty is, however, involved in the determination of the absolute number of hydrogen bonds which is strongly determined by the reference used.

The difference in the EPR parameters of MTSSL in methanol and ethanol might indicate that protic molecules larger than methanol are unable to establish a full hydrogen bond, perhaps due to steric hindrance induced by the methyl groups of the spin label or by the hydrophobic alkyl chains of the alcohols themselves. It would be interesting to compare our results with the computational approach used by Yagi and co-workers that involves a combination of Monte Carlo simulation and ab initio molecular orbital calculation with explicitly included solvent molecules to study the solvent effect on the electronic structure and A_{iso} of radicals.[31,32]

In the rigid-limit EPR spectra, A_{zz} is the dominating magnetic interaction instead of A_{iso} (cf. Figure 2a,b). A_{zz} is composed of $A_{zz} = A_{iso} + A_{zz,dip}$ (from eq 5), where $A_{zz,dip}$ is the dipolar coupling between electron and nuclear spin in the *z*-direction and is dominated by the spin density (ρ) in the p_z orbital at the nitrogen. The dipolar contribution is expected to be of the form $A_{zz,dip} = 2B$, $A_{xx,dip} = A_{yy,dip} = -B$, with $B = 4.8$ mT, where B is the magnitude of the dipolar interaction of the electron in the p_z orbital and the nuclear spin for $\rho = 1$. Empirically, A_{iso} can also be related to ρ by the McConnell relation $A_{iso} = Q\rho$, where the proportionality constant Q is in the order of 2.8 mT. (The effect of spin density in the p_z orbital of the oxygen atom of the NO fragment is significantly smaller (Q factor of 0.4 mT) and is therefore neglected.) This suggests that $A_{zz} = (Q + 2B)\rho$, i.e., $A_{zz} = (2.8 + 9.6\ \text{mT})\rho$.[44] From this estimate, A_{zz} should be more sensitive to changes in ρ and also follow the same dependence on the solvent polarity as A_{iso}. However, the empirical Q factor seems to overestimate the effect, as concluded from a study of many nitroxides by Ondar et al. which showed that $\Delta A_{zz}/\Delta A_{iso}$ is 2.3.[6,8] The same conclusion can be drawn from the X-band data from our study (Figures 4b and 5b).

Comparison of Figures 4a and 5a shows an overall agreement in the trends, but there is more scatter in the frozen solution X-band data compared to the liquid solution X-band data. Two factors must be taken into account to explain the differences: (1) Freezing of the solvents can change the hydrogen bonding situation. Indications of such effects are the large scatter in A_{zz} (within a region of 2 G) found for the MTSSL variants in the longer alcohols (1-butanol to 1-decanol, not included in Figure 5a), but more importantly, multiple freezing of a sample resulted in different A_{zz}-values, suggesting that the microenvironment of the spin label changes sufficiently to cause difference in A_{zz} (see section 5.2). Perhaps the aliphatic long alcohols are ordered in the vicinity of the spin label, thus creating a specific microenvironment which is sensitive to freezing conditions. The overall agreement of A_{zz} and A_{iso}, respectively, for MTSSL and MTSSL-β (Figures 4a and 5a) indicates the absence of solute-specific solvent cages.

(2) The temperature dependence of ϵ. For example, ϵ of ethanol increases from 24.3 at 25 °C to 41 at −60 °C.[36] However, a complete set of low-temperature ϵ-values, particularly for the temperature range where the measurements were made (77 K) is not available, and for that reason, the data in Figure 5 are plotted against room temperature ϵ-values. A similar correlation for room temperature and frozen solution data could therefore only be obtained if the temperature dependence of ϵ was the same for all solvents. This cannot be expected and could consequently be the origin of a part of the deviations seen between the data plotted in Figures 4 and 5.

The better resolution in W-band EPR spectra should allow to determine A_{zz} to greater accuracy. The general agreement of X- and W-band data is good (Figures 5 and 6), although the origin of the deviation of some of the A_{zz}- and ΔA_{zz}-values is not clear. Despite the sources of uncertainty described above, the propensity of the solvent to form hydrogen bonds to MTSSL is similar in the frozen solution as in the liquid solution (to be discussed further on). However, the most reliable comparison of experimental and calculated data appears to be made with the isotropic component of A_{iso}, obtained in liquid solution, although from a theoretical point of view, A_{iso} is more difficult to calculate (see above).

6.2. *g*-Tensor Components: g_{iso} and g_{xx}. The experimental results show that g_{iso} decreases with increasing ϵ of the solvent, and from the W-band EPR results, g_{xx} is identified as the dominant contribution to the solvent dependence (Figure 7). The dependence of g_{yy} on the solvent is smaller and g_{zz} is essentially solvent independent within the accuracy of the measurements. In several protic solvents, a second species with a larger g_{xx}-value was observed (see section 3.4). The g_{xx}-value of this species is similar to g_{xx} in the most apolar, aprotic solvents (e.g., toluene). This indicates that the additional contribution is due to spin labels with less hydrogen bonds than the majority conformation. Previously, a varying degree of hydrogen bonding in spin labels has been suggested by Ondar et al.[6] and Earle et al.[7] To compare the solvent dependence of g_{iso} with that of the W-band data, we use $g_{iso} = (g_{xx} + g_{yy} + g_{zz})/3$. Regarding g_{yy} and g_{zz} as solvent independent, the spread in g_{iso} should be a third of the spread in g_{xx}, which is in agreement with the experiments.

An increased solvent polarity shifts spin density from the oxygen to the nitrogen within the NO bond. The formation of hydrogen bonds affects the spin label *g*-tensor parameters via three separate effects: (1) Transfer of spin density from the oxygen to the nitrogen atom, (2) increase of the $n\pi^*$ excitation energy, resulting in a lower g_{xx}-value, and (3) transfer of some electron density from the lone-pair orbitals at the NO oxygen to the hydrogen donated in the hydrogen bond. This has been shown earlier in several studies employing various nitroxide spin labels in different environments.[3−9,11,12,33]

Due to limitations in the computational DFT methods, the calculation of *g*-values performed here is restricted to hydrogen bonding effects. As discussed for the calculation of hyperfine parameters, models A−C are defined comprising zero to two hydrogen bonded water molecules. In a separate study of the influence of hydrogen bonding on the *g*-tensor of spin labels, calculated with ROHF reference states, we found that the ROHF method exaggerated the effect of hydrogen bonded water molecules.[12] Our present results show that more accurate *g*-value shifts can be obtained with DFT methods (compare DFT data,

$\Delta g_{xx}^{AB} = -0.00044$ and $\Delta g_{xx}^{BC} = -0.00038$ (Table 2) with ROHF data, $\Delta g_{xx}^{AB} = -0.0021$ and $\Delta g_{xx}^{BC} = -0.0018$, from Engström et al.[12]). This improvement is primarily due to the inclusion of electron correlation through the DFT functionals. To be able to account for changes in the dielectric properties of the solvents in the *g*-value calculations as well, further theoretical development of the DFT method is needed.

Qualitative comparisons of MTSSL data with the results of DFT calculations (Tables 1 and 2) show that the decrease in g_{iso} from methanol to water (−0.00023) matches well the contribution calculated for a hydrogen bond (−0.00015). The decrease in g_{iso} from toluene to methanol (−0.00020) also matches one hydrogen bond (−0.00017). Note, however, that the difference in ϵ of these two solvents is not considered in the calculations, suggesting that the change in g_{iso} due to hydrogen bonding are somewhat overestimated by the DFT models. Previously, g_{iso} for the DTBNO radical was found to decrease by 0.00023 from methanol to water and by 0.00027 from toluene to methanol,[3] i.e., in close agreement with our MTSSL data. The experimental anisotropic g_{xx}-value decreases by 0.00057 from toluene to methanol, to be compared with a decrease of 0.00044 due to one hydrogen bond. In similarity with the situation for g_{iso}, this underestimation of the shift can be due to the exclusion of the effect of ϵ. Water and methanol have a smaller difference in g_{xx} (−0.00012) than the calculated contribution of a second hydrogen bond (−0.00038). This could be due to a difference in the hydrogen bonding situation in the frozen and in the liquid state of the sample, or it could indicate that the DFT method overestimates the effect of hydrogen bonding on g_{xx}. The former interpretation is more likely since the shift in g_{iso} from methanol to water is larger than the calculated shift due to a second hydrogen bond (Figure 7). This is further supported by the hyperfine parameters discussed above, where the increase in ΔA_{iso} from methanol to water is larger than the calculated value for the difference between one and two hydrogen bonds (Figure 4b), whereas the increase in ΔA_{zz} from frozen solvents at X-band is smaller than the calculated increase due to a second hydrogen bond (Figure 5b). The uncertainty of the W-band A_{zz}-value in water is too large to be included in the comparison (Figure 6). Somewhat different shifts in g_{xx} to lower values were found for the NO-15 spin label (Reanal, Hungary) compared to our values for MTSSL, −0.00093 from toluene to methanol, and −0.00026 from methanol to water.[5]

Overall, both with respect to the hyperfine coupling and the *g*-tensor parameters, the DFT method reflects the solvent effects over a wide range of solvent polarities and proticities. Hence, the calculations can be used to get a molecular picture of the effects of the solvent on the dissolved spin label.

6.3. Correlation of Hyperfine Coupling and *g*-Tensor Parameters. Figure 8 shows the correlation between the hyperfine and *g*-tensor parameters as determined experimentally. A linear correlation is expected from the dependence of *g* and *A* on solvent properties, as demonstrated in several earlier studies using other spin labels.[3−7,11] For the isotropic parameters, g_{iso} and A_{iso}, Figure 8 shows a linear correlation with some scatter. A larger scatter is found for the anisotropic parameters, g_{xx} and A_{zz}, which were taken from the W-band EPR data (see sections 5.2 and 5.3). The intrinsically higher resolution of W-band EPR in combination with the higher sensitivity of g_{xx} and A_{zz} compared to g_{iso} and A_{iso} to the environment of the spin label suggest that the scatter is not due to random error but, rather, reflects the different mechanisms by which the solvent properties affect the *g*- and hyperfine coupling tensors, in particular the differences between protic and aprotic solvents (see above and Kawamura et al.[3]). We therefore propose that there are two linear correlations with different slopes reflecting the protic and aprotic solvents, respectively. Given the small number of data points, the statistical basis for this statement is poor, but we suggest that the dotted lines shown in Figure 8 have a diagnostic value and reflect the polarity/proticity properties of the environment. Previously, a classification into aprotic and protic local environments of spin-labeled proteins was made from the arrangement of anisotropic data in such a plot.[7,11]

6.4. Comparison with Spin-Labeled Proteins. To illustrate one of the practical applications of the present investigation, we compare the anisotropic solvent data (A_{zz} and g_{xx}) of MTSSL obtained to a recent investigation by Steinhoff and co-workers, in which bacteriorhodopsin was labeled with MTSSL along the ion channel.[11] A_{zz} varied from 35.0 to 36.7 G, depending on whether MTSSL was situated in the cytoplasmic region near the chromophore retinal (site 46) or on the extracellular surface (site 129), respectively.[11] The polarity and proticity of various local regions in proteins are different and these properties are likely comparable to those of isotropic solvents. According to our data (Table 1), the local environment of the inner cytoplasmic region has similar properties as ethanol, i.e., an ϵ of 20−25 and a minor probability of hydrogen bonding. On the other hand, at the extracellular surface MTSSL probes an environment similar to that of water, which shows that MTSSL is accessible to the aqueous buffer. Between these extremes, A_{zz} shifts gradually due to the water density gradient of the ion channel. They also observed a decrease in g_{xx} of ∼0.00035 between the cytoplasmic and extracellular sites, which (from our W-band solvent data) nicely indicates the same environmental shift ($\Delta g_{xx}^{ethanol,water} = -0.00035$; Table 1).

7. Conclusions

We have shown that the parameters A_{iso}, g_{iso}, A_{zz}, and g_{xx} of MTSSL are sensitive to aprotic and protic solvents with ϵ-values ranging from 2.4 to 109. The higher resolution of W-band EPR allows to determine most of the anisotropic observables of the nitroxide. Thus, in comparison to X-band EPR, the method is more sensitive to the properties of the environment of the spin label. DFT methods can be used to calculate shifts in the *A*-values due to changed dielectric and hydrogen bonding properties, as well as shifts in *g*-values due to hydrogen bonding. A combined qualitative analysis of experimental and calculated data makes it possible to interpret the parameter shifts as due to the changed ϵ and/or the increased propensity for hydrogen bonding. Thus, for aprotic solvents and all alcohols except methanol ($\epsilon < 25$), the shifts in A_{iso} and A_{zz} are proportional to the change in ϵ, whereas the shifts between solvents with polar ($\epsilon > 25$) and protic properties are dominated by their different degrees of proticity. Our analysis suggests, for example, that methanol forms ∼1 and water ∼2 hydrogen bonds to MTSSL in average. We found that the DFT method predicts the influence of hydrogen bonding on the *g*-values with a larger accuracy than the ROHF method. We have also shown how the anisotropic solvent data can be used as a "ruler" to interpret rigid-limit data from spin-labeled proteins in terms of environmental properties, i.e., polarity and proticity.

Acknowledgment. We thank Hans Borén for excellent technical assistance and valuable discussions concerning the GC-MS experiments and analysis and Maria Fittipaldi for enthusiastic assistance in the W-band EPR measurements. We also thank Juha Vaara and Bernd Schimmelpfennig for their support

in the *g*-tensor calculations. Edgar Groenen and Jan Schmidt are acknowledged for providing support for the work performed in Leiden. We thank Antoine Wolff, Andreas Kamlowski, and Peter Höfer (Bruker, Germany) for technical support. This work was supported by grants from the Foundation for Strategic Research (R.O. and M.E.) and the Swedish Natural Science Research Council (M.L.). The W-band EPR measurements in Leiden were performed under the auspices of the BIOMAC Research School of the Leiden and Delft Universities and was supported with financial aid by The Netherlands Organization of Scientific Research (NWO), department of Chemical Sciences (CW).

References and Notes

(1) Berliner, L. J.; Reuben, J. *Biological Magnetic Resonance, Vol. 8: Spin Labeling - Theory and Applications*; Plenum Press: New York, 1989.

(2) Hubbell, W. L.; Gross, A.; Langen, R.; Lietzov, M. A. *Curr. Opin. Struct. Biol.* **1998**, *8*, 649.

(3) Kawamura, T.; Matsunami, S.; Yonezawa, T. *Bull. Chem. Soc. Jpn.* **1967**, *40*, 1111.

(4) Griffith, O. H.; Dehlinger, P. J.; Van, S. P. *J. Membr. Biol.* **1974**, *15*, 159.

(5) Krinichnyi, V. I.; Grinberg, O. Y.; Bogatyrenko, V. R.; Likhtenshtein, G. I.; Lebedev, Y. S. *Biophysics* **1985**, *30*, 233.

(6) Ondar, M. A.; Grinberg, O. Y.; Dubinskii, A. A.; Lebedev, Y. S. *Sov. J. Chem. Phys.* **1985**, *3*, 781.

(7) Earle, K. A.; Moscicki, J. K.; Ge, M.; Budil, D. E.; Freed, J. H. *Biophys. J.* **1994**, *66*, 1213.

(8) Ondar, M. A.; Grinberg, O. Y.; Dubinskii, A. A.; Shestakov, A. F.; Lebedev, Y. S. *Sov. J. Chem. Phys.* **1985**, *2*, 83.

(9) Krinichnyi, V. I.; Grinberg, O. Y.; Yudanova, Y. I.; Lyubashevskaya, Y. V.; Antsiferova, L. I.; Likhtenshtein, G. I.; Lebedev, Y. S. *Biophysics* **1987**, *32*, 229.

(10) Steinhoff, H. J.; Pfeiffer, M.; Rink, T.; Burlon, O.; Kurz, M.; Riesle, J.; Heuberger, E.; Gerwert, K.; Oesterhelt, D. *Biophys. J.* **1999**, *76*, 2702.

(11) Steinhoff, H. J.; Savitsky, A.; Wegener, C.; Pfeiffer, M.; Plato, M.; Möbius, K. *Biochim. Biophys. Acta* **2000**, *1457*, 253.

(12) Engström, M.; Owenius, R.; Vahtras, O. *Chem. Phys. Lett.* **2001**, *338*, 407.

(13) Eriksson, L. A. *Mol. Phys.* **1997**, *91*, 827.

(14) Himo, F.; Gräslund, A.; Eriksson, L. A. *Biophys. J.* **1997**, *72*, 1556.

(15) Adamo, C.; di Matteo, A.; Rey, P.; Barone, V. *J. Phys. Chem. A* **1999**, *103*, 3481.

(16) Rega, N.; Cossi, M.; Barone, V. *J. Chem. Phys.* **1996**, *105*, 11060.

(17) Burghaus, O.; Plato, M.; Rohrer, M.; Möbius, K.; MacMillan, F.; Lubitz, W. *J. Phys. Chem.* **1993**, *97*, 7639.

(18) Knüpling, M.; Törring, J. T.; Un, S. *Chem. Phys.* **1997**, *219*, 291.

(19) Törring, J. T.; Un, S.; Knüpling, M.; Plato, M.; Möbius, K. *J. Chem. Phys.* **1997**, *107*, 3905.

(20) van Lenthe, E.; Wormer, P. E. S.; van der Avoird, A. *J. Chem. Phys.* **1997**, *107*, 2488.

(21) Schreckenbach, G.; Ziegler, T. *Theor. Chem. Acc.* **1998**, *99*, 71.

(22) Malkina, O. L.; Vaara, J.; Schimmelpfennig, B.; Munzarova, M.; Malkin, V. G.; Kaupp, M. *J. Am. Chem. Soc.* **2000**, *122*, 9206.

(23) Lushington, G. H.; Grein, F. *J. Chem. Phys.* **1997**, *106*, 3292.

(24) Jayatilaka, D. *J. Chem. Phys.* **1998**, *108*, 7587.

(25) Vahtras, O.; Minaev, B.; Ågren, H. *Chem. Phys. Lett.* **1997**, *281*, 186.

(26) Mustafaev, S. A.; Schastnev, P. V. *J. Struct. Chem.* **1989**, *30*, 582.

(27) Harriman, J. E. *Theoretical Foundations of Electron Spin Resonance*; Academic Press: New York, 1978.

(28) Onsager, L. *J. Am. Chem. Soc.* **1936**, *58*, 1486.

(29) Reddoch, A. H.; Konishi, S. *J. Chem. Phys.* **1979**, *70*, 2121.

(30) Al-Bala'a, I.; Bates, D., Jr. *J. Magn. Reson.* **1987**, *73*, 78.

(31) Yagi, T.; Takase, H.; Morihashi, K.; Kikuchi, O. *Chem. Phys.* **1998**, *232*, 1.

(32) Yagi, T.; Kikuchi, O. *J. Phys. Chem. A* **1999**, *103*, 9132.

(33) Kawamura, T.; Matsunami, S.; Yonezawa, T.; Fukui, K. *Bull. Chem. Soc. Jpn.* **1965**, *38*, 1935.

(34) Stone, A. J. *Mol. Phys.* **1963**, *6*, 509.

(35) Stone, A. J. *Mol. Phys.* **1964**, *7*, 311.

(36) Weast, R. C. *CRC Handbook of Chemistry and Physics*, 64th ed.; CRC Press: Boca Raton, 1983; pp E49−E52.

(37) Frisch, M. J.; Trucks, G. W.; Schlegel, H. B.; Scuseria, G. E.; Robb, M. A.; Cheeseman, J. R.; Zakrzewski, V. G.; Montgomery, J. A., Jr.; Stratmann, R. E.; Burant, J. C.; Dapprich, S.; Millam, J. M.; Daniels, A. D.; Kudin, K. N.; Strain, M. C.; Farkas, O.; Tomasi, J.; Barone, V.; Cossi, M.; Cammi, R.; Mennucci, B.; Pomelli, C.; Adamo, C.; Clifford, S.; Ochterski, J.; Petersson, G. A.; Ayala, P. Y.; Cui, Q.; Morokuma, K.; Malick, D. K.; Rabuck, A. D.; Raghavachari, K.; Foresman, J. B.; Cioslowski, J.; Ortiz, J. V.; Stefanov, B. B.; Liu, G.; Liashenko, A.; Piskorz, P.; Komaromi, I.; Gomperts, R.; Martin, R. L.; Fox, D. J.; Keith, T.; Al-Laham, M. A.; Peng, C. Y.; Nanayakkara, A.; Gonzalez, C.; Challacombe, M.; Gill, P. M. W.; Johnson, B.; Chen, W.; Wong, M. W.; Andres, J. L.; Gonzalez, C.; Head-Gordon, M.; Replogle, E. S.; Pople, J. A. *Gaussian 98*, Revision A.5; Gaussian, Inc.: Pittsburgh, PA, 1998.

(38) Salahub, D. R.; Fournier, R.; Mlynarski, P.; Papai, I.; St-Amant, A.; Ushio, J. In *Density Functional Methods in Chemistry*; Labanowski, J. K., Andzelm, J. W., Eds.; Springer-Verlag: New York, 1991; pp 77−100.

(39) Kutzelnigg, W.; Fleischer, U.; Schindler, M. *NMR - Basic Principles and Progress*; Springer-Verlag: Heidelberg, 1990; Vol. 23.

(40) Pipek, J.; Mezey, P. G. *J. Chem. Phys.* **1989**, *90*, 4916.

(41) Hess, B. A.; Marian, C. M.; Wahlgren, U.; Gropen, O. *Chem. Phys. Lett.* **1996**, *251*, 365.

(42) Schimmelpfennig, B. *Atomic Spin-Orbit Mean-Field Integral Program*; Stockholm University: Stockholm, Sweden, 1996.

(43) Symons, M. C. R.; Pena-Nuñes, A. S. *J. Chem. Soc., Faraday Trans. 1* **1985**, *81*, 2421.

(44) Weil, J. A.; Bolton, J. R.; Wertz, J. E. *Electron Paramagnetic Resonance. Elementary Theory and Practical Applications*; John Wiley & Sons: New York, 1994; p 256.